

**Synthetic, Structural, and Luminescent Study of Uranyl Coordination Polymers
Containing Chelating Terpyridine and Trispyridyltriazine Ligands**

Sonia G. Thangavelu^a, Simon J. A. Pope^b, and Christopher L. Cahill^{a*}

^a Department of Chemistry, The George Washington University, 800 22nd Street, NW,
Washington, DC, 20052, USA

^b School of Chemistry, Main Building, Cardiff University, Cardiff, Cymru/Wales, UK,
CF10 3AT

*Corresponding author. Phone: (202) 994-6959. Email: cahill@gwu.edu

Supporting Information

Table S1. Selected bond lengths (\AA) and bond angles ($^\circ$) for the uranyl centers in **1**.

U(1)-O(2)	1.766(4)
U(1)-O(1)	1.773(4)
U(1)-O(4)	2.269(4)
U(1)-O(6)	2.276(4)
U(1)-N(1)	2.577(5)
U(1)-N(3)	2.582(5)
U(1)-N(2)	2.592(5)
O(2)-U(1)-O(1)	177.44(18)
O(2)-U(1)-O(4)	90.18(16)
O(1)-U(1)-O(4)	92.37(17)
O(2)-U(1)-O(6)	89.88(17)
O(1)-U(1)-O(6)	90.73(16)
O(4)-U(1)-O(6)	80.55(14)
O(2)-U(1)-N(1)	87.94(17)
O(1)-U(1)-N(1)	89.72(17)

O(4)-U(1)-N(1)	160.45(15)
O(6)-U(1)-N(1)	79.99(15)
O(2)-U(1)-N(3)	86.38(17)
O(1)-U(1)-N(3)	94.10(16)
O(4)-U(1)-N(3)	75.00(15)
O(6)-U(1)-N(3)	155.23(15)
N(1)-U(1)-N(3)	124.25(15)
O(2)-U(1)-N(2)	96.53(17)
O(1)-U(1)-N(2)	81.49(16)
O(4)-U(1)-N(2)	136.22(15)
O(6)-U(1)-N(2)	142.35(14)
N(1)-U(1)-N(2)	63.29(15)
N(3)-U(1)-N(2)	62.41(15)

Table S2. Selected bond lengths (\AA) and bond angles ($^\circ$) for the uranyl centers in **2**.

U(1)-O(1)	1.7676(18)
U(1)-O(2)	1.7781(18)
U(1)-O(6)	2.2724(19)
U(1)-O(4)	2.2762(18)
U(1)-N(3)	2.576(2)
U(1)-N(1)	2.583(2)
U(1)-N(2)	2.592(2)
O(1)-U(1)-O(2)	177.37(9)
O(1)-U(1)-O(6)	89.86(8)
O(2)-U(1)-O(6)	92.75(8)
O(1)-U(1)-O(4)	90.74(8)
O(2)-U(1)-O(4)	80.35(7)
O(1)-U(1)-N(3)	87.79(8)

O(2)-U(1)-N(3)	89.84(8)
O(6)-U(1)-N(3)	160.26(7)
O(4)-U(1)-N(3)	80.05(7)
O(1)-U(1)-N(1)	86.70(8)
O(2)-U(1)-N(1)	93.71(8)
O(6)-U(1)-N(1)	75.11(7)
O(4)-U(1)-N(1)	155.23(7)
N(3)-U(1)-N(1)	124.26(7)
O(1)-U(1)-N(2)	96.54(8)
O(2)-U(1)-N(2)	81.37(7)
O(6)-U(1)-N(2)	136.59(7)
O(4)-U(1)-N(2)	142.20(7)
N(3)-U(1)-N(2)	63.14(7)
N(1)-U(1)-N(2)	62.54(7)

Table S3. Selected bond lengths (\AA) and bond angles ($^\circ$) for the uranyl centers in **3**.

U(1)-O(2)	1.750(5)
U(1)-O(1)	1.760(6)
U(1)-O(4)	2.246(5)
U(1)-O(5)	2.313(5)
U(1)-N(6)	2.575(6)
U(1)-N(2)	2.585(5)
U(1)-N(1)	2.605(5)
O(2)-U(1)-O(1)	175.1(2)
O(2)-U(1)-O(4)	90.5(2)
O(1)-U(1)-O(4)	93.2(2)
O(2)-U(1)-O(5)	90.4(2)
O(1)-U(1)-O(5)	93.3(2)

O(4)-U(1)-O(5)	81.06(19)
O(2)-U(1)-N(6)	90.8(2)
O(1)-U(1)-N(6)	86.9(2)
O(4)-U(1)-N(6)	159.65(18)
O(5)-U(1)-N(6)	78.62(18)
O(2)-U(1)-N(2)	82.90(19)
O(1)-U(1)-N(2)	92.2(2)
O(4)-U(1)-N(2)	137.84(18)
O(5)-U(1)-N(2)	140.24(18)
N(6)-U(1)-N(2)	62.41(17)
O(2)-U(1)-N(1)	91.5(2)
O(1)-U(1)-N(1)	86.2(2)
O(4)-U(1)-N(1)	76.89(17)
O(5)-U(1)-N(1)	157.88(18)
N(6)-U(1)-N(1)	123.37(16)
N(2)-U(1)-N(1)	61.81(16)

Table S4. Selected bond lengths (\AA) and bond angles ($^\circ$) for the uranyl centers in **4**.

U(1)-O(2)	1.753(4)
U(1)-O(1)	1.763(4)
U(1)-O(6)#1	2.257(4)
U(1)-O(3)	2.301(4)
U(1)-N(2)	2.569(4)
U(1)-N(1)	2.592(5)
U(1)-N(3)	2.606(5)
O(2)-U(1)-O(1)	176.97(18)
O(2)-U(1)-O(6)#1	91.47(18)
O(1)-U(1)-O(6)#1	89.20(16)

O(2)-U(1)-O(3)	89.32(17)
O(1)-U(1)-O(3)	93.70(16)
O(6)#1-U(1)-O(3)	82.09(14)
O(2)-U(1)-N(2)	81.98(16)
O(1)-U(1)-N(2)	95.59(16)
O(6)#1-U(1)-N(2)	138.98(15)
O(3)-U(1)-N(2)	137.82(14)
O(2)-U(1)-N(1)	94.82(17)
O(1)-U(1)-N(1)	85.59(16)
O(6)#1-U(1)-N(1)	158.68(15)
O(3)-U(1)-N(1)	77.64(14)
N(2)-U(1)-N(1)	62.24(14)
O(2)-U(1)-N(3)	91.21(17)
O(1)-U(1)-N(3)	86.04(16)
O(6)#1-U(1)-N(3)	78.04(14)
O(3)-U(1)-N(3)	160.13(14)
N(2)-U(1)-N(3)	61.77(14)
N(1)-U(1)-N(3)	122.07(14)

Table S5. Selected bond lengths (\AA) and bond angles ($^\circ$) for the uranyl centers in **5**.

U(1)-O(2)	1.750(6)
U(1)-O(1)	1.755(6)
U(1)-O(5)	2.245(6)
U(1)-O(3)	2.280(5)
U(1)-N(2)	2.597(6)
U(1)-N(1)	2.615(6)
U(1)-N(3)	2.637(7)
O(2)-U(1)-O(1)	176.0(3)

O(2)-U(1)-O(5)	93.9(3)
O(1)-U(1)-O(5)	89.6(3)
O(2)-U(1)-O(3)	91.4(2)
O(1)-U(1)-O(3)	91.0(2)
O(5)-U(1)-O(3)	81.9(2)
O(2)-U(1)-N(2)	91.4(2)
O(1)-U(1)-N(2)	84.7(2)
O(5)-U(1)-N(2)	138.1(2)
O(3)-U(1)-N(2)	139.6(2)
O(2)-U(1)-N(1)	84.3(2)
O(1)-U(1)-N(1)	94.6(2)
O(5)-U(1)-N(1)	77.6(2)
O(3)-U(1)-N(1)	158.6(2)
N(2)-U(1)-N(1)	61.59(19)
O(2)-U(1)-N(3)	90.8(2)
O(1)-U(1)-N(3)	86.5(3)
O(5)-U(1)-N(3)	159.5(2)
O(3)-U(1)-N(3)	78.1(2)
N(2)-U(1)-N(3)	61.56(19)
N(1)-U(1)-N(3)	122.75(19)

Table S6. Selected bond lengths (\AA) and bond angles ($^\circ$) for the uranyl centers in **6**.

U(1)-O(1)	1.742(5)
U(1)-O(2)	1.747(5)
U(1)-O(4)	2.234(4)
U(1)-O(5)	2.308(5)
U(1)-N(2)	2.586(5)
U(1)-N(1)	2.600(5)

U(1)-N(3)	2.617(5)
O(1)-U(1)-O(2)	175.40(19)
O(1)-U(1)-O(4)	90.2(2)
O(2)-U(1)-O(4)	93.1(2)
O(1)-U(1)-O(5)	90.8(2)
O(2)-U(1)-O(5)	92.9(2)
O(4)-U(1)-O(5)	81.03(18)
O(1)-U(1)-N(2)	83.38(19)
O(2)-U(1)-N(2)	92.02(19)
O(4)-U(1)-N(2)	137.66(17)
O(5)-U(1)-N(2)	140.58(17)
O(1)-U(1)-N(1)	91.3(2)
O(2)-U(1)-N(1)	86.7(2)
O(4)-U(1)-N(1)	160.14(18)
O(5)-U(1)-N(1)	79.14(17)
N(2)-U(1)-N(1)	62.13(16)
O(1)-U(1)-N(3)	91.2(2)
O(2)-U(1)-N(3)	86.4(2)
O(4)-U(1)-N(3)	76.65(17)
O(5)-U(1)-N(3)	157.60(17)
N(2)-U(1)-N(3)	61.78(15)
N(1)-U(1)-N(3)	123.10(15)

Table S7. Selected bond lengths (\AA) and bond angles ($^\circ$) for the uranyl centers in **7**.

U(1)-O(2)	1.744(3)
U(1)-O(1)	1.756(3)
U(1)-O(3)	2.259(3)
U(1)-O(6)#1	2.278(3)

U(1)-N(2)	2.572(3)
U(1)-N(6)	2.596(4)
U(1)-N(1)	2.628(3)
O(1)-U(1)-O(2)	177.01(13)
O(2)-U(1)-O(3)	89.04(13)
O(1)-U(1)-O(3)	91.99(13)
O(2)-U(1)-O(6)#1	96.13(14)
O(1)-U(1)-O(6)#1	86.81(13)
O(3)-U(1)-O(6)#1	81.07(11)
O(2)-U(1)-N(2)	94.24(13)
O(1)-U(1)-N(2)	83.18(12)
O(3)-U(1)-N(1)	140.24(11)
O(6)#1-U(1)-N(2)	137.53(11)
O(2)-U(1)-N(6)	88.31(13)
O(1)-U(1)-N(6)	89.15(13)
O(3)-U(1)-N(6)	78.53(11)
O(6)#1-U(1)-N(6)	159.05(11)
N(2)-U(1)-N(6)	62.01(1)
O(2)-U(1)-N(1)	87.09(13)
O(1)-U(1)-N(1)	92.99(12)
O(3)-U(1)-N(1)	157.79(11)
O(6)#1-U(1)-N(1)	77.61(11)
N(2)-U(1)-N(1)	61.92(11)
N(6)-U(1)-N(1)	123.16(10)

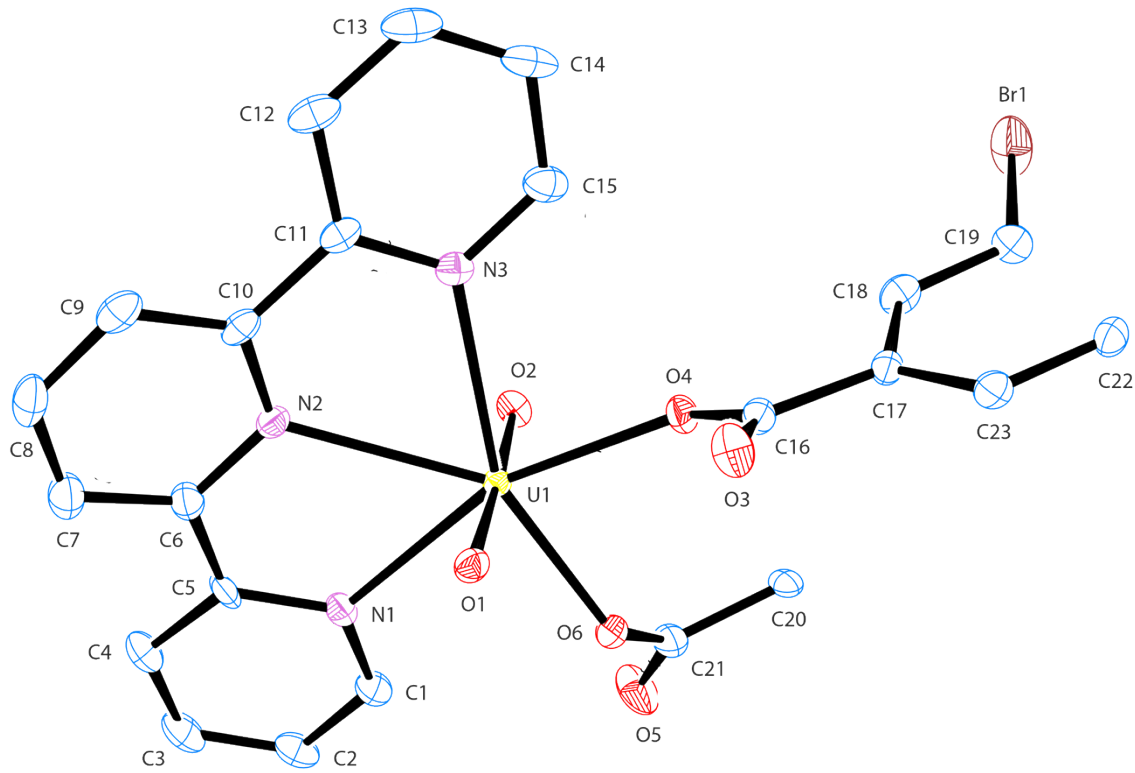


Figure S1. The ORTEP diagram of **1** [$(\text{UO}_2)(\text{BrC}_8\text{H}_3\text{O}_4)(\text{C}_{15}\text{H}_{11}\text{N}_3)$]. Thermal ellipsoids are shown at 50% probability level. Hydrogens have been omitted.

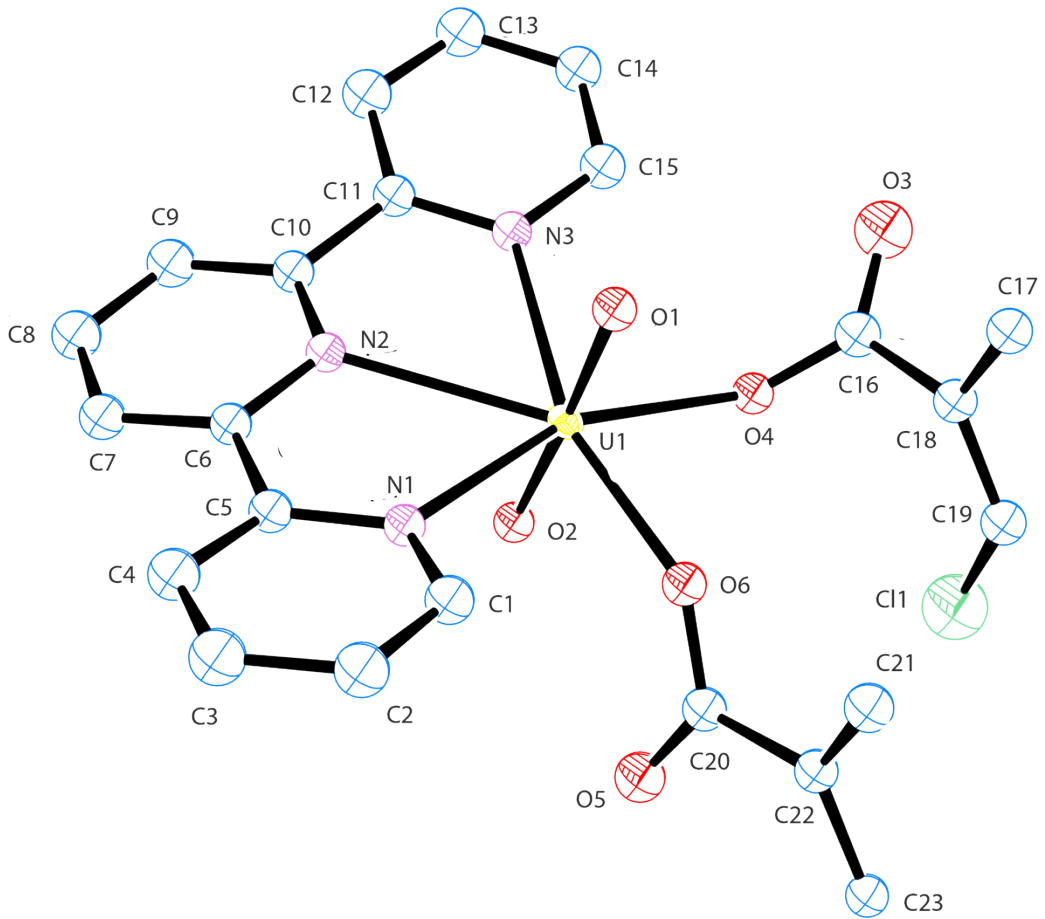


Figure S2. The ORTEP diagram of **2** [$(\text{UO}_2)(\text{ClC}_8\text{H}_3\text{O}_4)(\text{C}_{15}\text{H}_{11}\text{N}_3)$]. Thermal ellipsoids are shown at 50% probability level. Hydrogens have been omitted.

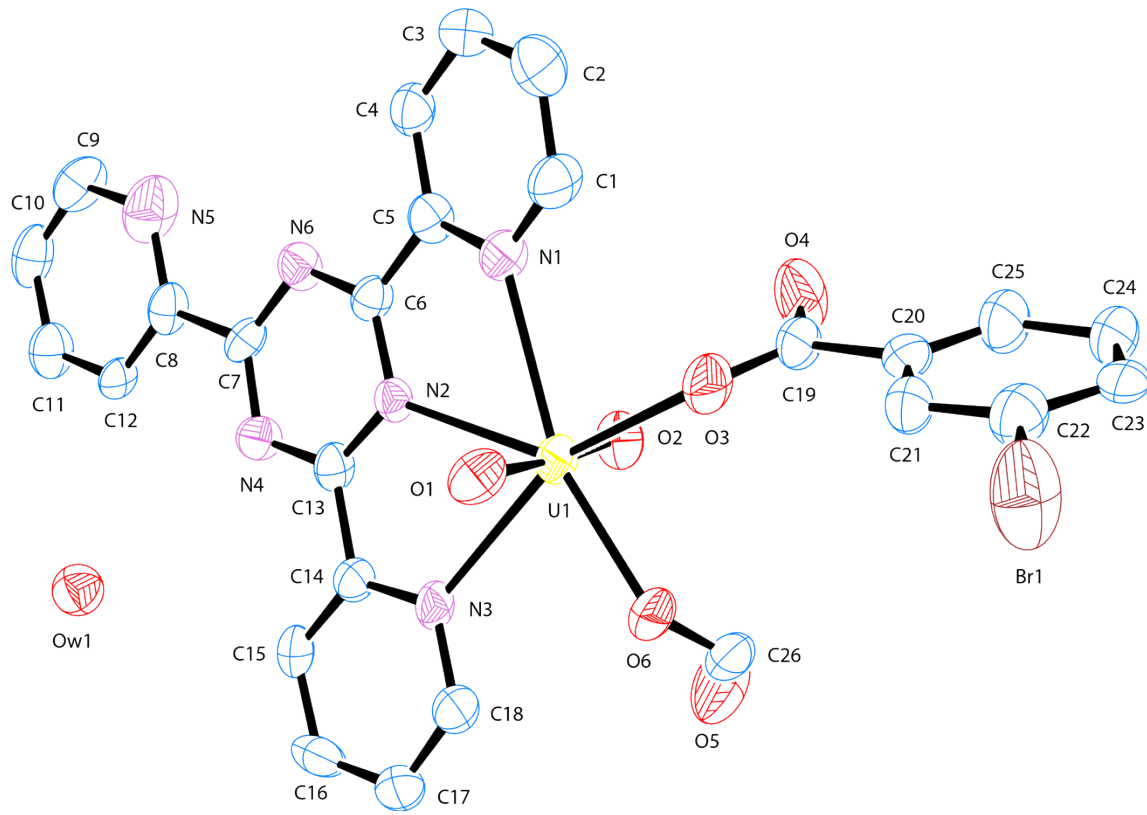


Figure S3. The ORTEP diagram of **3** $[(\text{UO}_2)(\text{BrC}_8\text{H}_3\text{O}_4)(\text{C}_{18}\text{H}_{12}\text{N}_6)] \cdot \text{H}_2\text{O}$. Thermal ellipsoids are shown at 50% probability level. Hydrogens have been omitted.

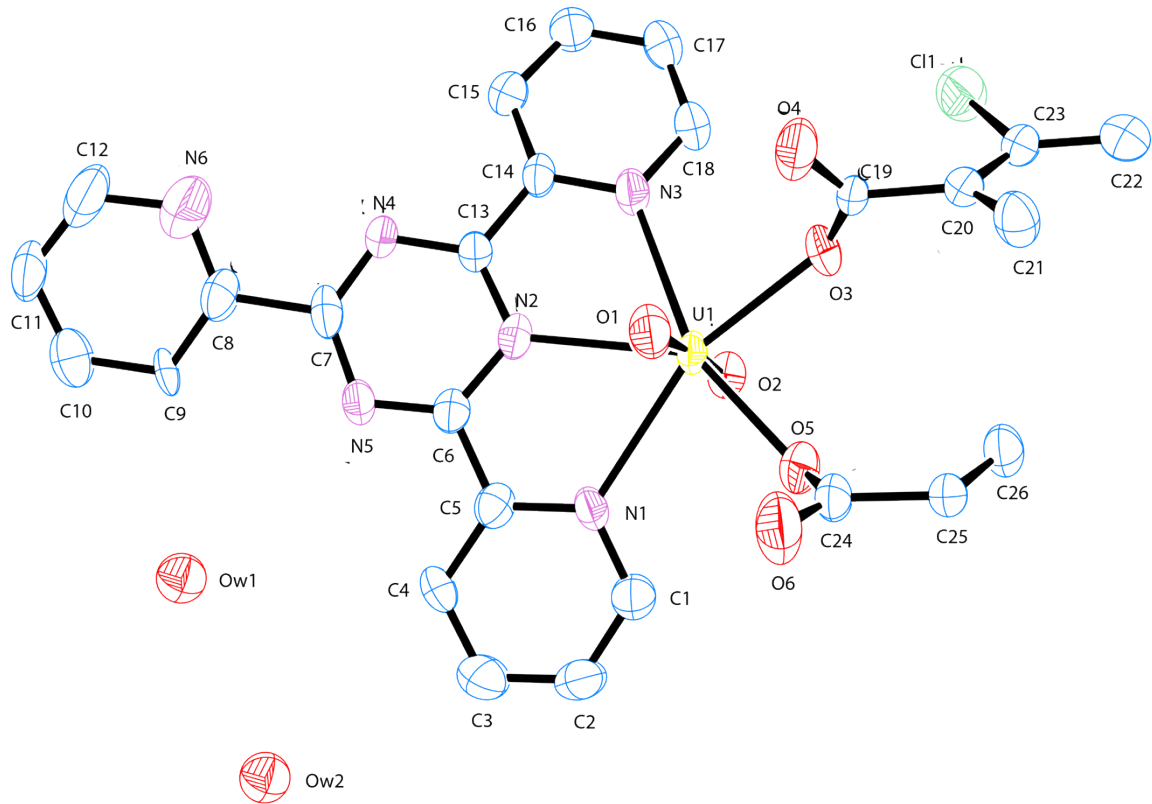


Figure S4. The ORTEP diagram of **4** $[(\text{UO}_2)(\text{ClC}_8\text{H}_3\text{O}_4)(\text{C}_{18}\text{H}_{12}\text{N}_6)] \cdot 2\text{H}_2\text{O}$. Thermal ellipsoids are shown at 50% probability level. Hydrogens have been omitted.

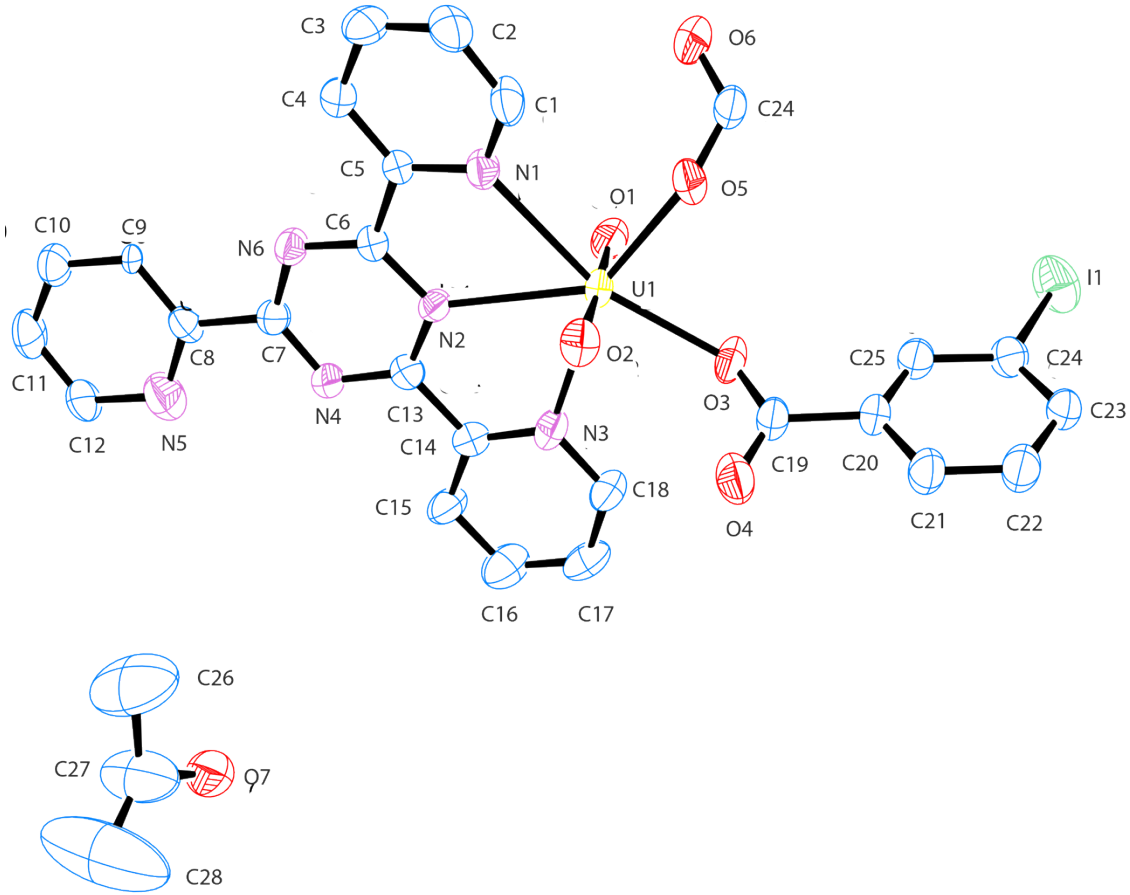


Figure S5. The ORTEP diagram of **5** $[(\text{UO}_2)(\text{C}_8\text{H}_3\text{IO}_4)(\text{C}_{18}\text{H}_{12}\text{N}_6)] \cdot 2\text{C}_3\text{H}_7\text{O}$. Thermal ellipsoids are shown at 50% probability level. Hydrogens have been omitted.

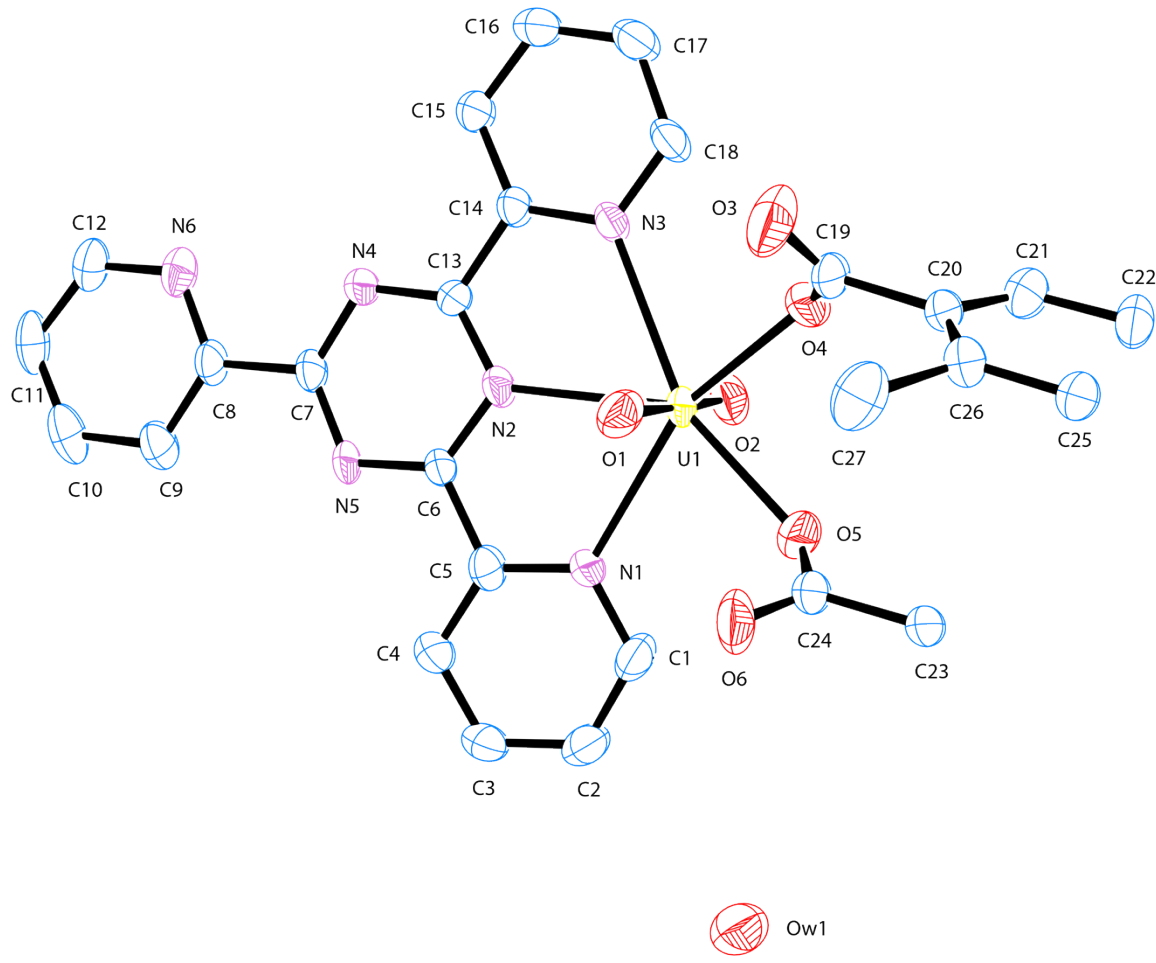


Figure S6. The ORTEP diagram of **6** $[(\text{UO}_2)(\text{C}_9\text{H}_6\text{O}_4)(\text{C}_{18}\text{H}_{12}\text{N}_6)] \cdot \text{H}_2\text{O}$. Thermal ellipsoids are shown at 50% probability level. Hydrogens have been omitted.

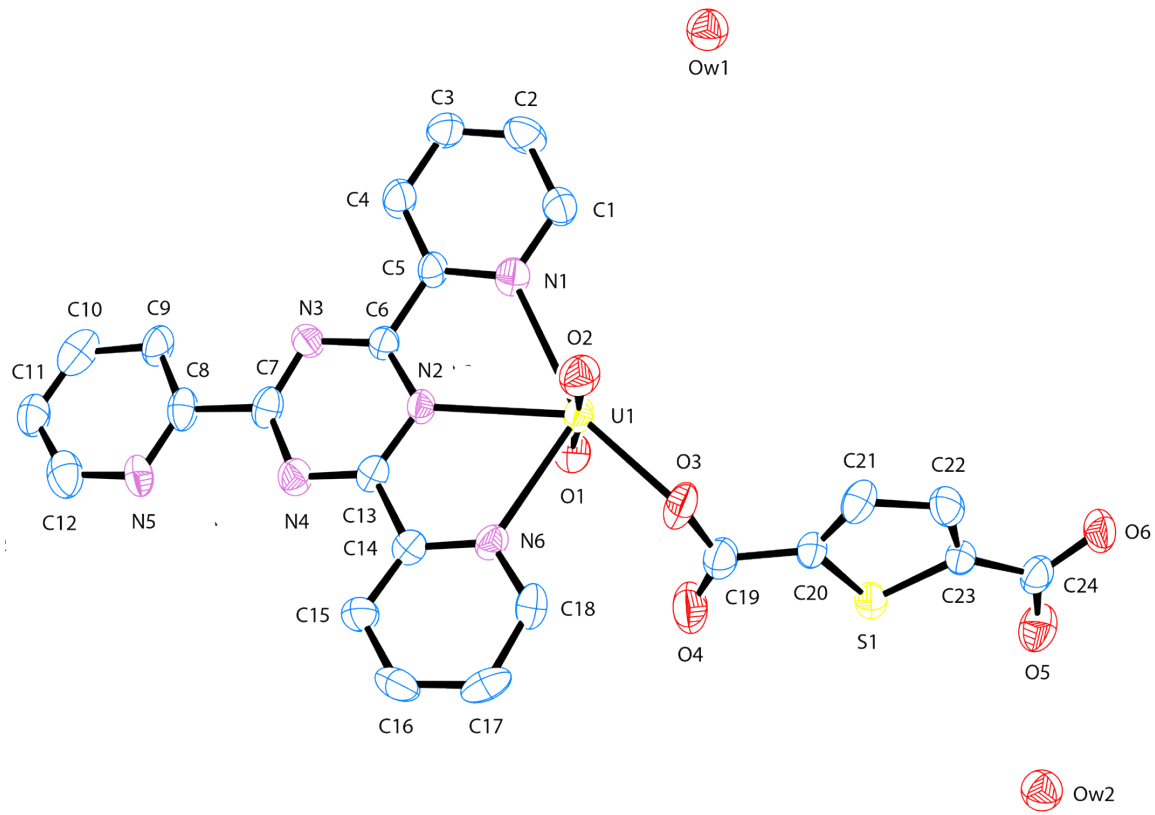


Figure S7. The ORTEP diagram of **7** $[(\text{UO}_2)(\text{C}_6\text{H}_2\text{O}_4\text{S})(\text{C}_{18}\text{H}_{12}\text{N}_6)] \cdot 2\text{H}_2\text{O}$. Thermal ellipsoids are shown at 50% probability level. Hydrogens have been omitted.

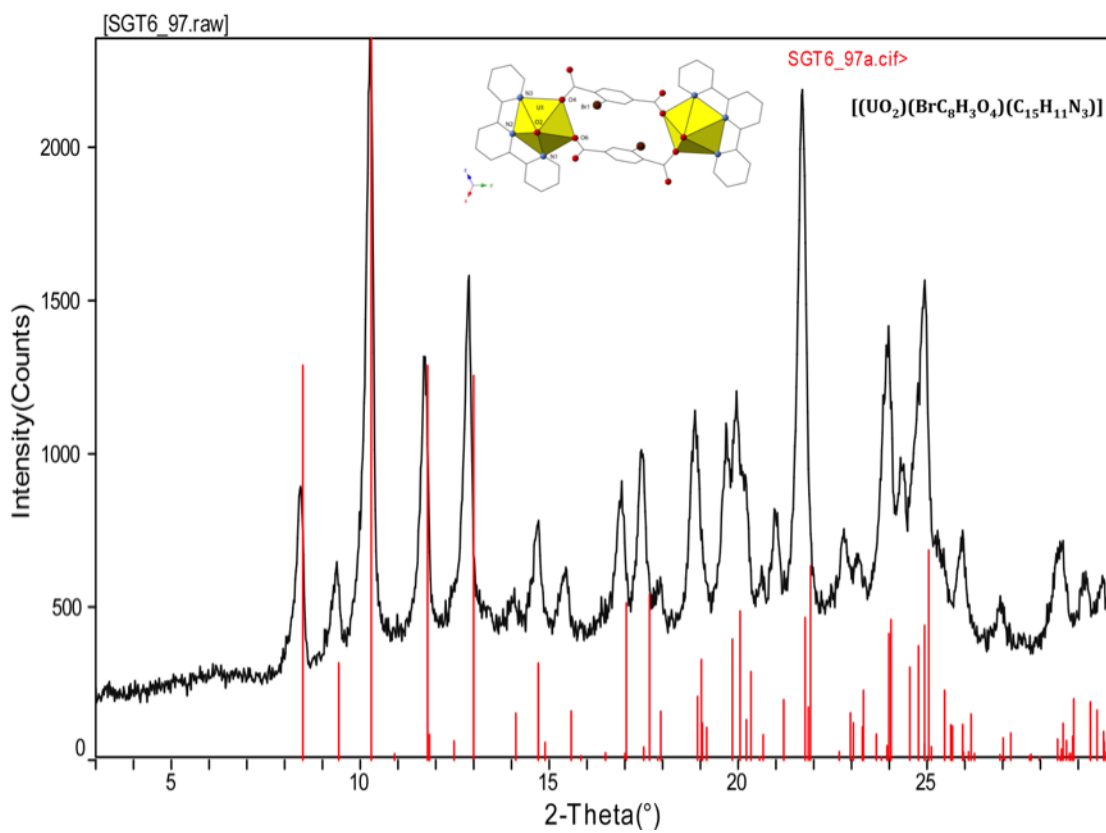


Figure S8. Observed and calculated powder X-ray diffraction pattern for **1**.

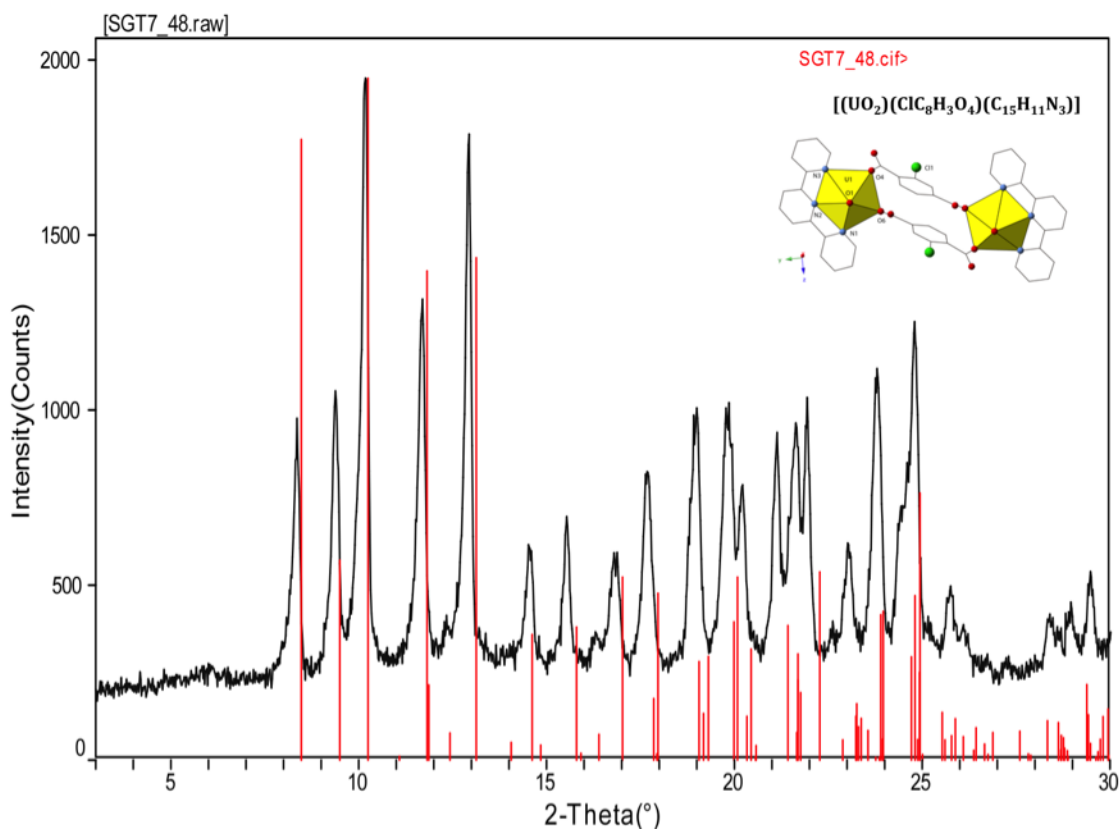


Figure S9. Observed and calculated powder X-ray diffraction pattern for **2**.

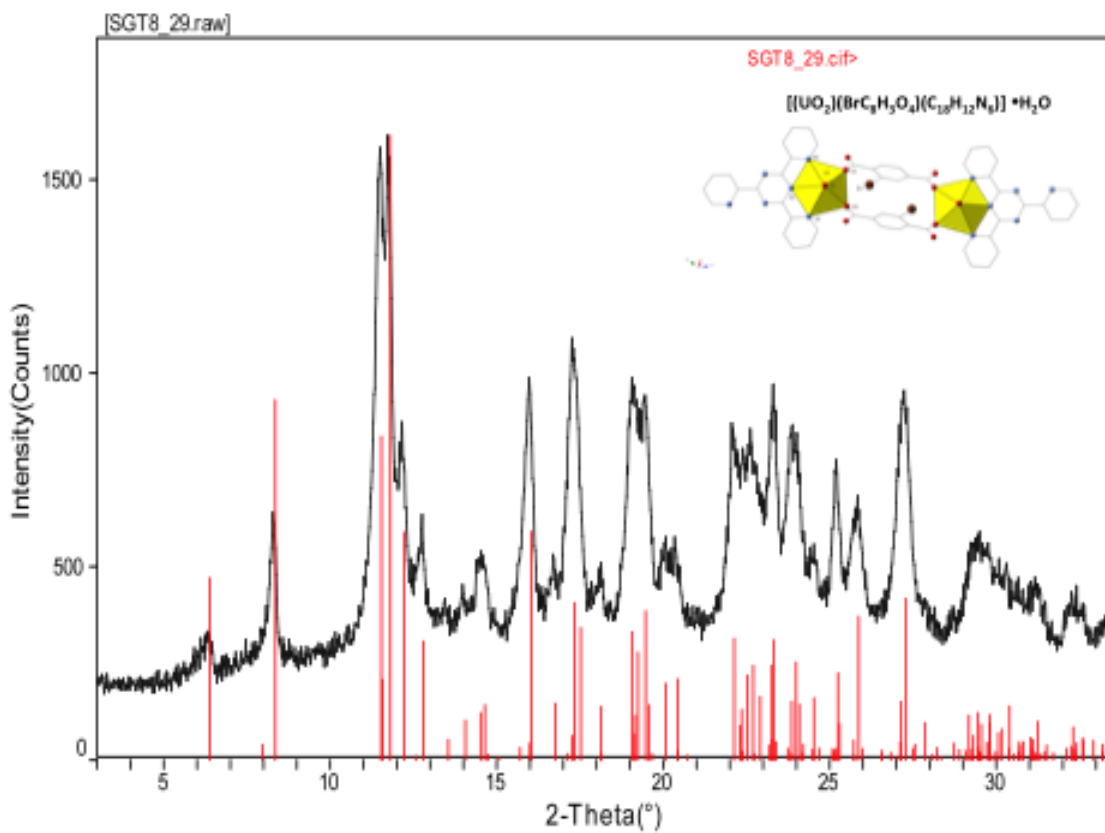


Figure S10. Observed and calculated powder X-ray diffraction pattern for **3**.

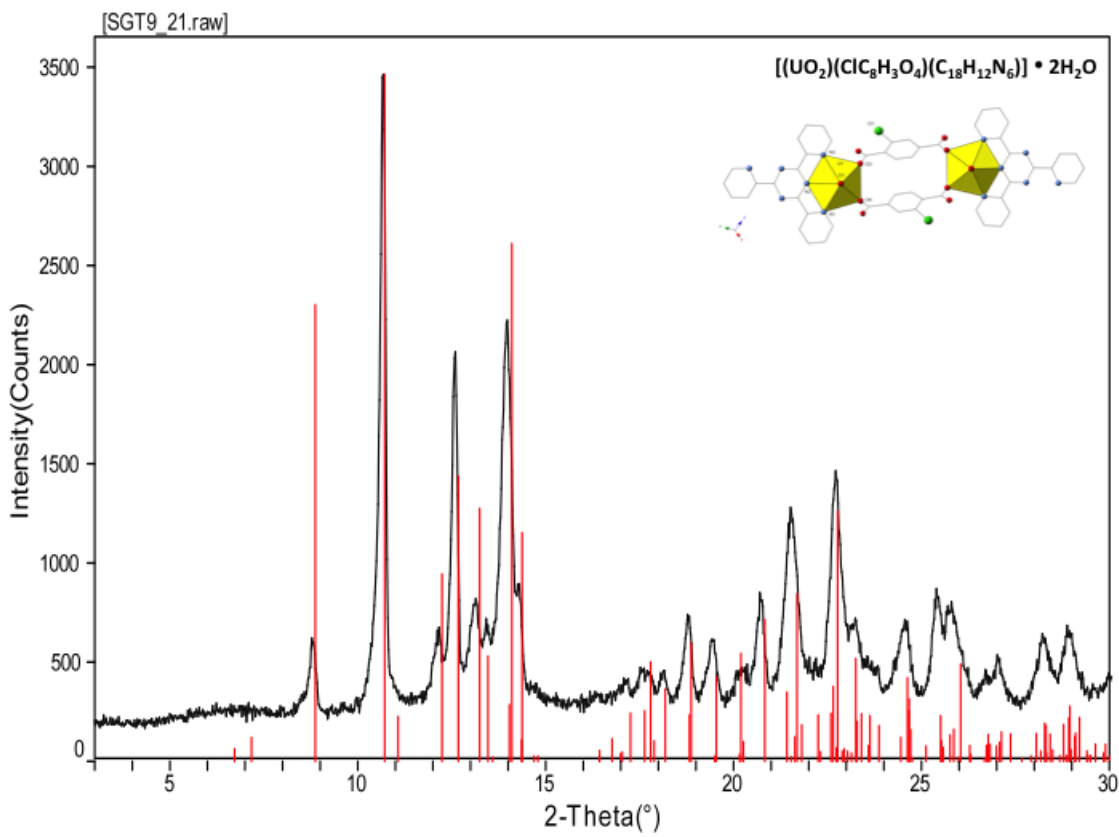


Figure S11. Observed and calculated powder X-ray diffraction pattern for **4**.

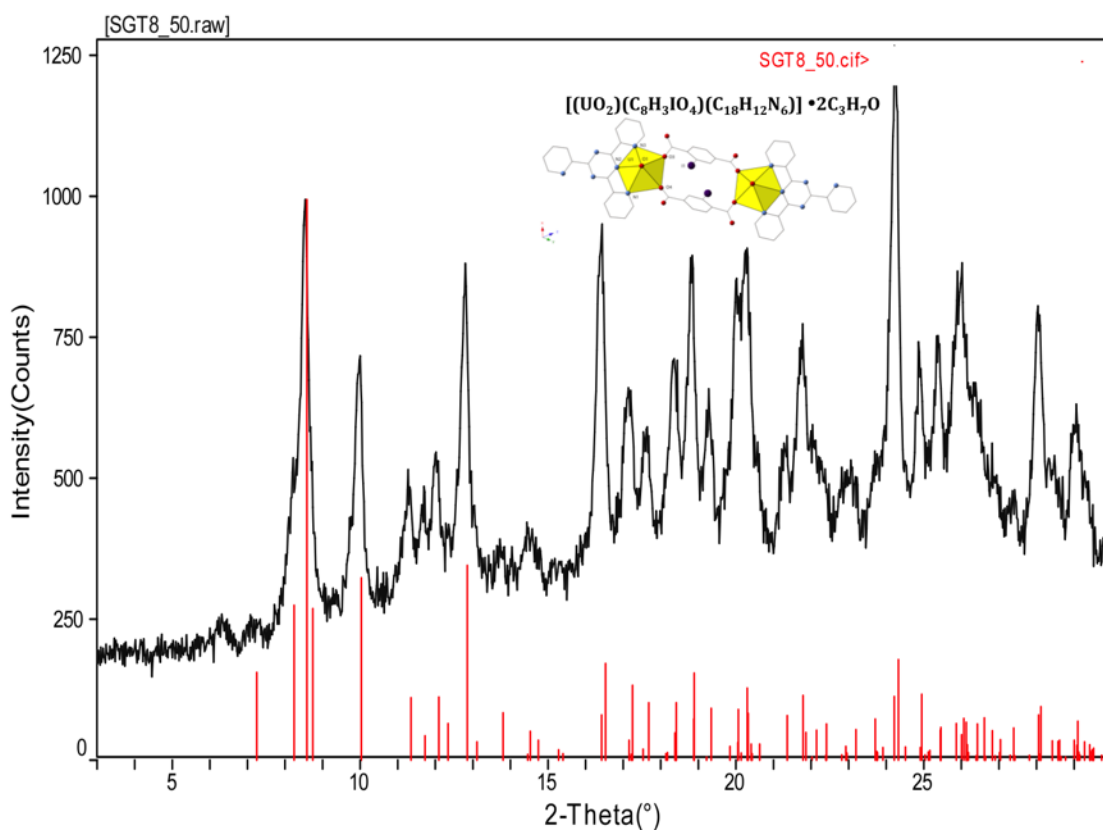


Figure S12. Observed and calculated powder X-ray diffraction pattern for **5**.

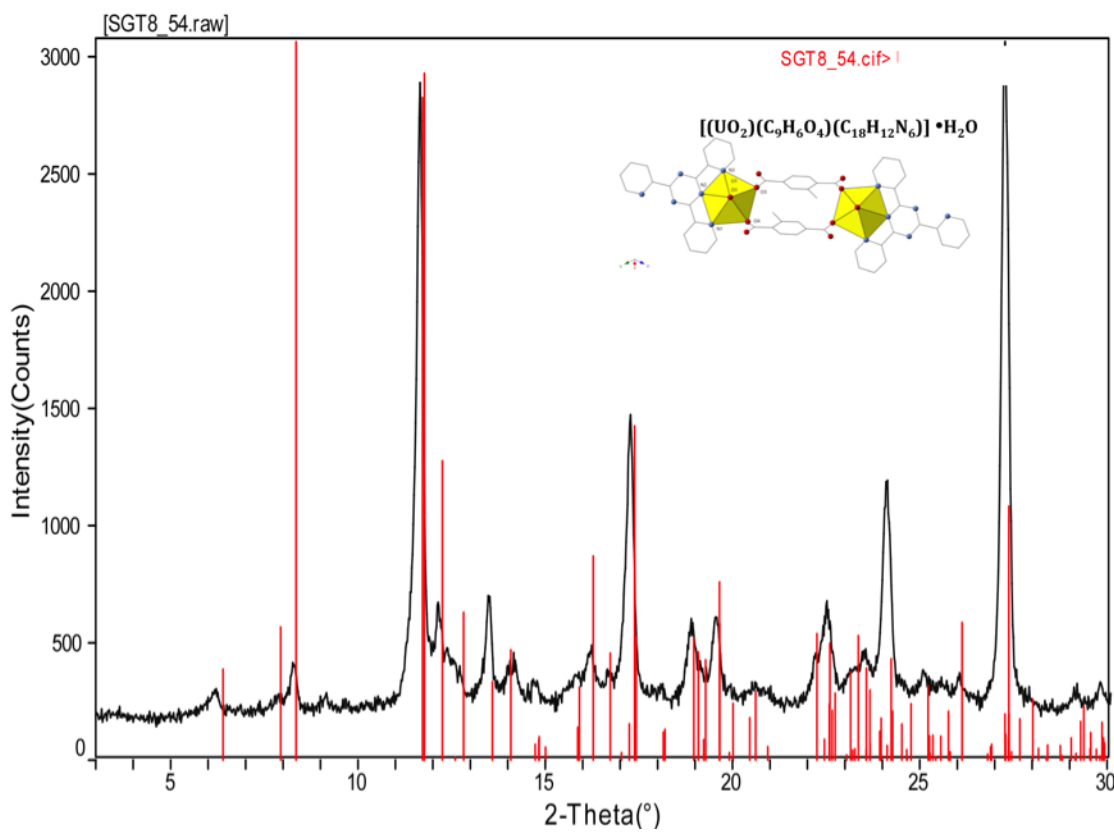


Figure S13. Observed and calculated powder X-ray diffraction pattern for **6**.

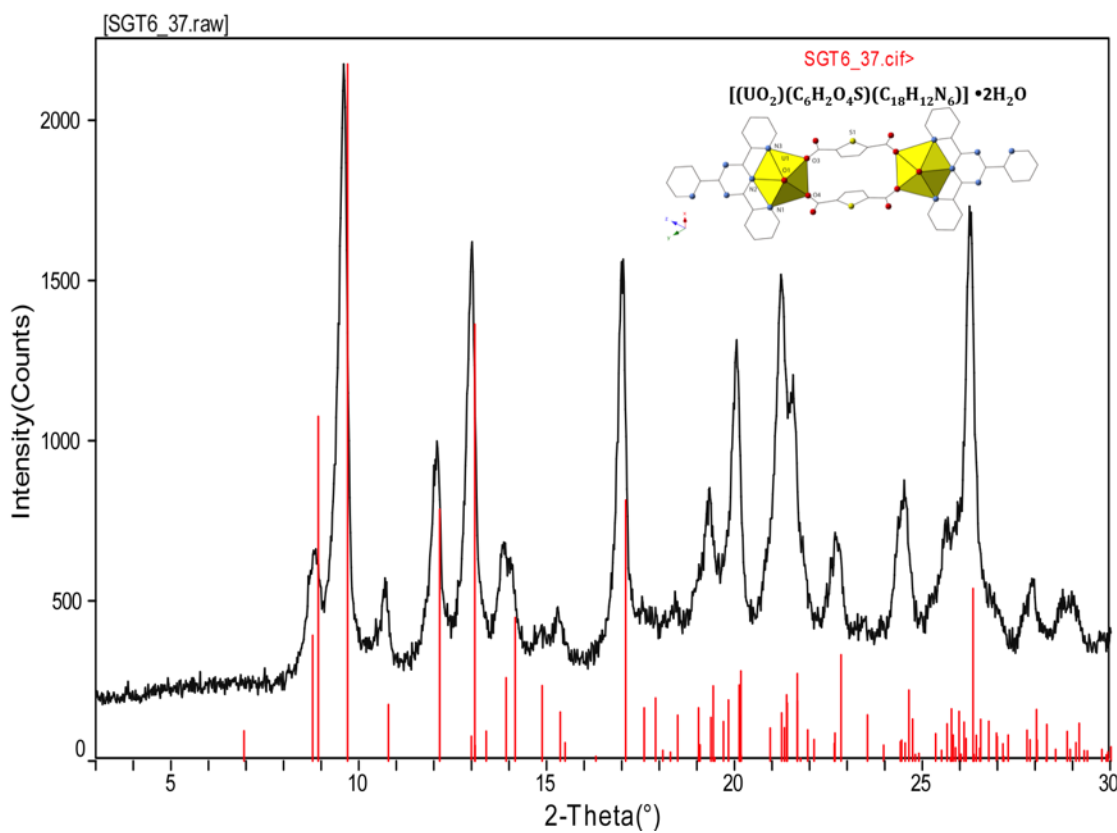


Figure S14. Observed and calculated powder X-ray diffraction pattern for **7**.

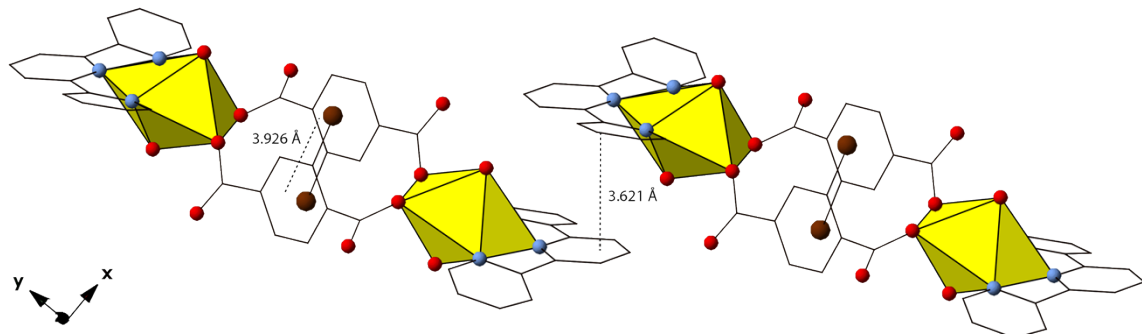


Figure S15. The packing diagram of **1**. Weak π - π interactions are observed between two Br-BDC rings and TPY ligands of adjacent dimers.

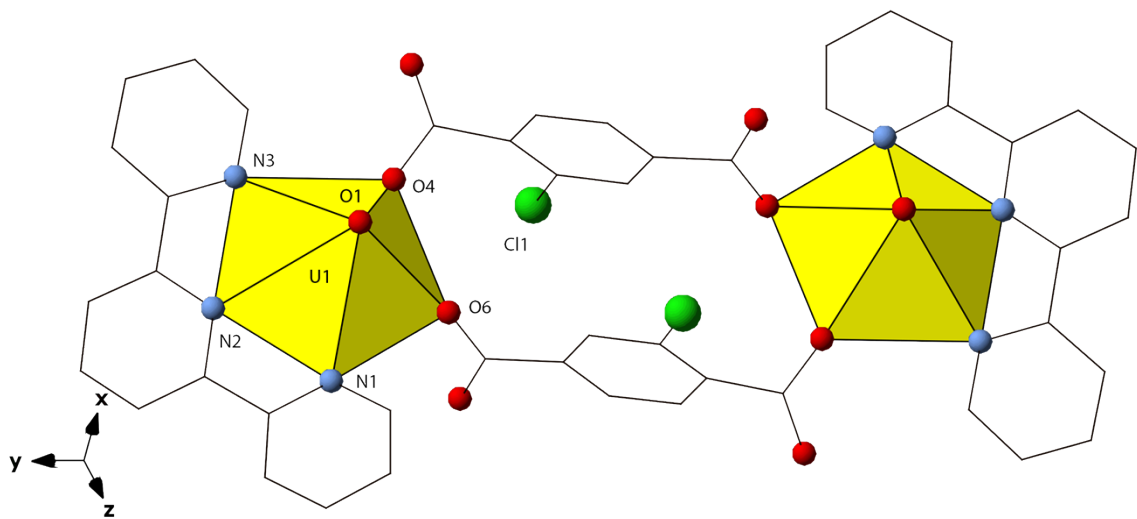


Figure S16. The crystal structure of **2**.

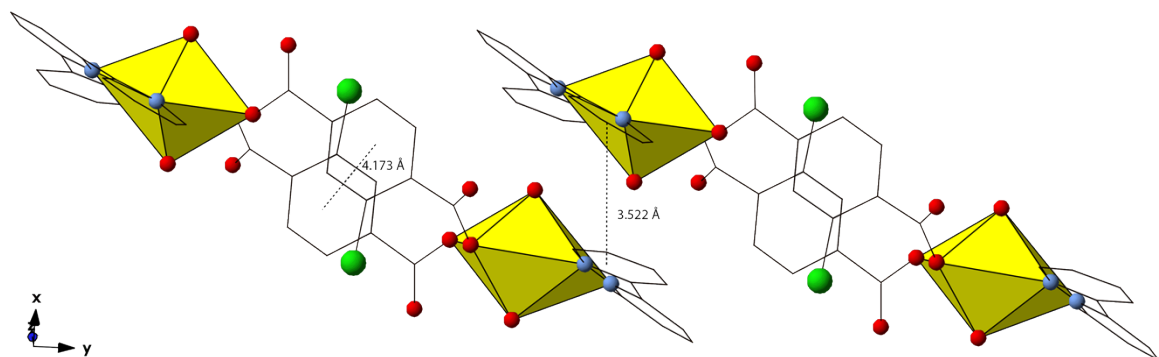


Figure S17. The packing diagram of **2**.

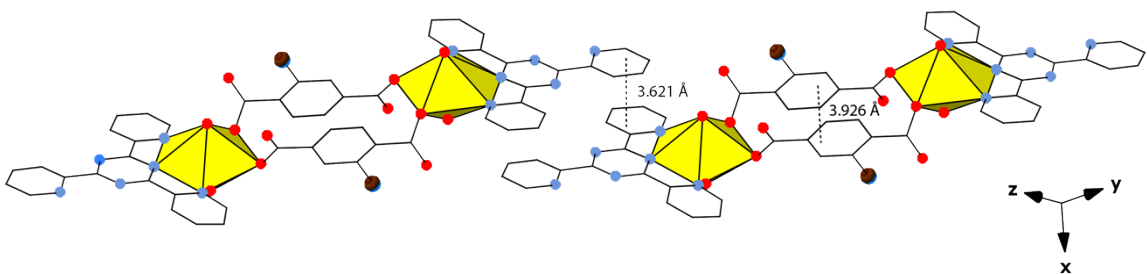


Figure S18. The packing diagram of **3**. The two π - π interactions are observed between two Br-BDC rings and between TPTZ ligands of adjacent dimers.

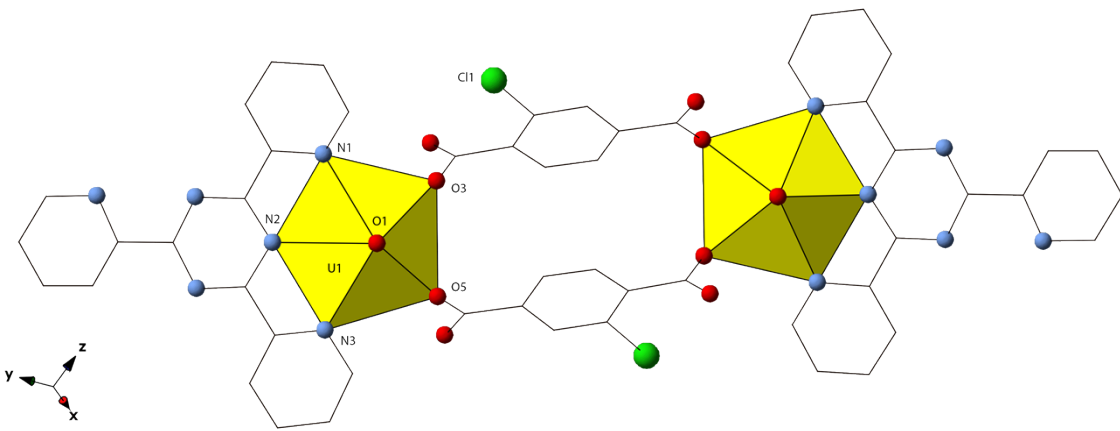


Figure S19. The crystal structure of **4**.

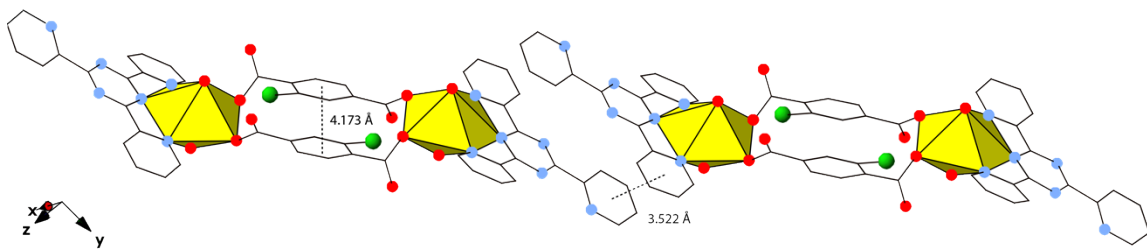


Figure S20. The packing diagram of **4**.

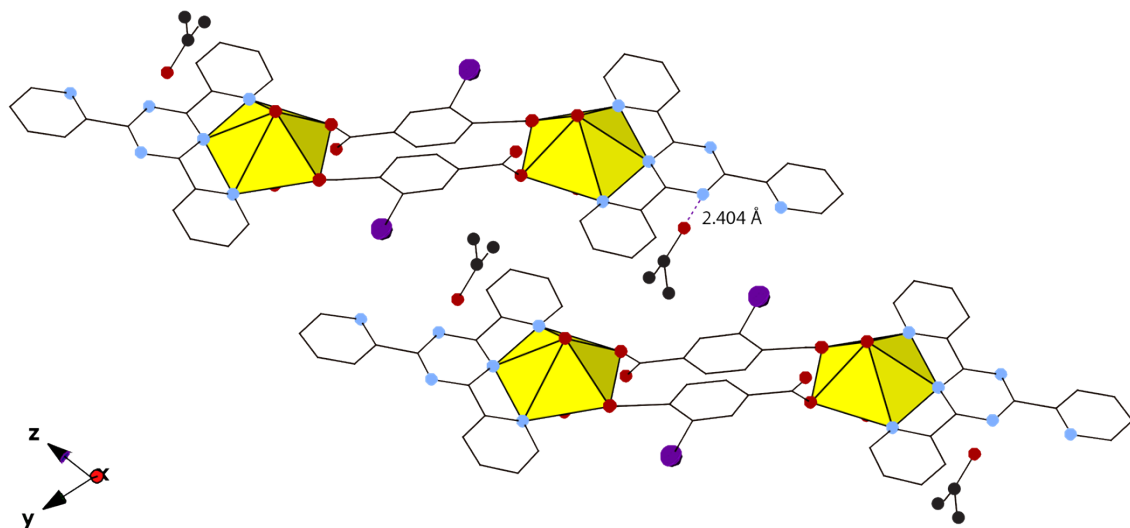


Figure S21. The packing diagram of **5**. The hydroxyl proton of 2-propanol participates in hydrogen bonding with the nitrogen atom in the pyrazyl ring of TPTZ. Black spheres represent carbon.

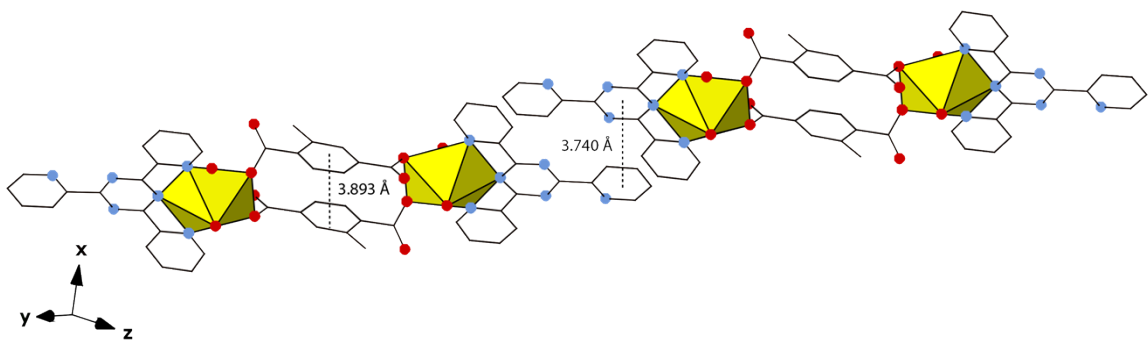


Figure S22. The packing diagram of **6**. π - π interactions are observed between two Me-BDC rings and between TPTZ ligands of adjacent dimers.

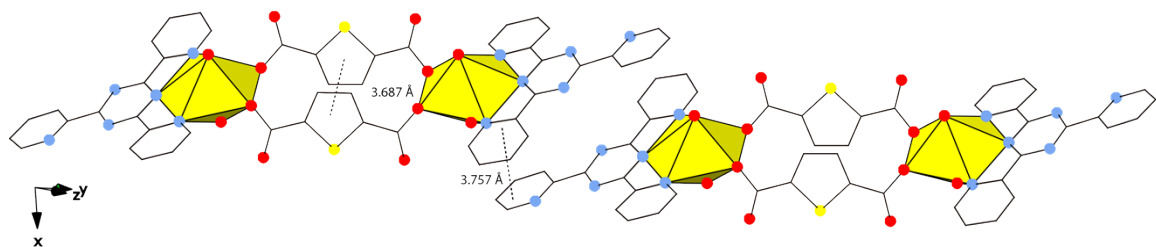


Figure S23. The packing diagram of **7**.

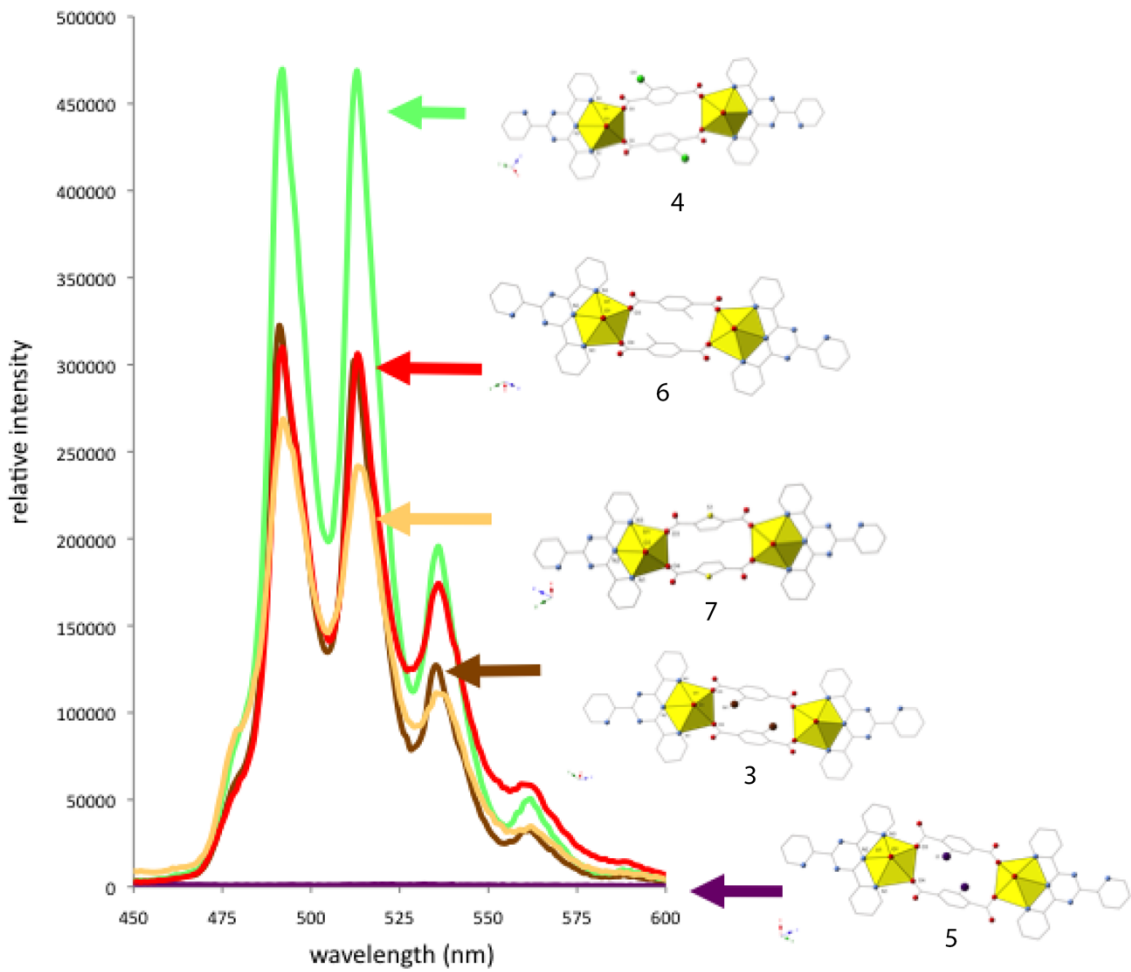


Figure S24. Solid-state emission spectra of **3-7** (excitation: 365 nm, 298 K).

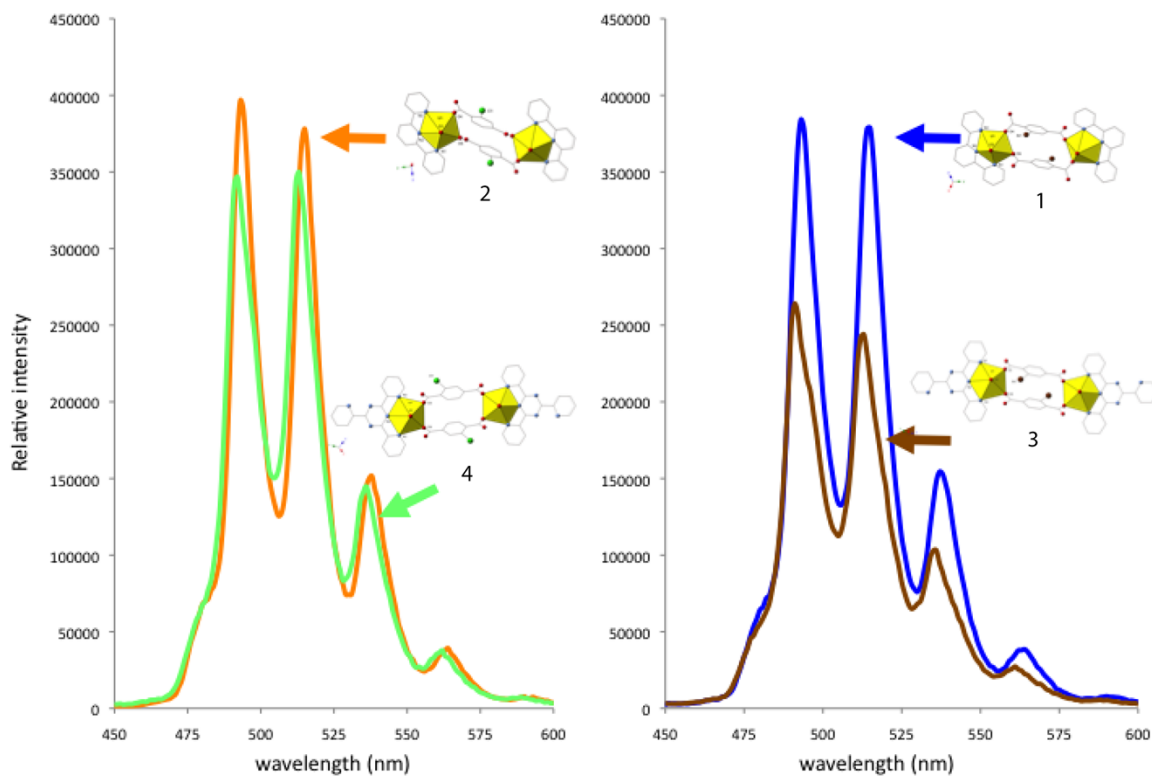


Figure S25. Solid-state emission spectra of **1-4** (excitation: 365 nm, 298 K).

General Determination of Emission Shift. To determine the emission shifts of **1-4**, the peak positions of each spectrum were measured. The peak positions of **1** and **3** were superimposed to the emission peak positions of **2** and **4** respectively and then the energy difference between each peak was calculated. A summary of these results can be found in Tables S8 and S9.

Table S8. Summary of emission peak positions and shifts of **1** and **3** at 365 nm.

Compound	Position 1 (cm ⁻¹)	Position 2 (cm ⁻¹)	Position 3 (cm ⁻¹)	Position 4 (cm ⁻¹)	Average (cm ⁻¹)
3	20364	19531	18692	17889	19119
1	20284	19455	18622	17794	19039
Energy shift	80	76	70	95	80

Table S9. Summary of emission peak positions and shifts of **2** and **4** at 365 nm.

Compound	Position 1 (cm ⁻¹)	Position 2 (cm ⁻¹)	Position 3 (cm ⁻¹)	Position 4 (cm ⁻¹)	Average (cm ⁻¹)
4	20325	19493	18692	17825	19084
2	20284	19417	18622	17794	19029
Energy shift	41	76	70	31	55

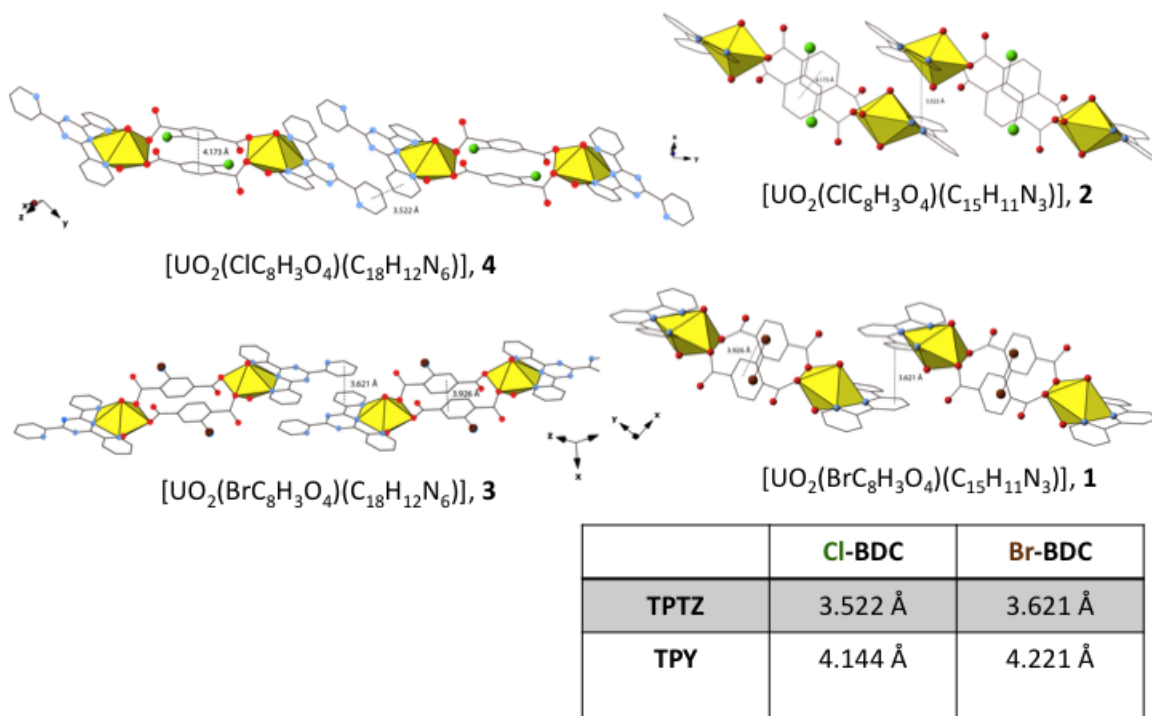


Figure S26. A comparison of π -stacking distances of adjacent N-donor ligands in **1-4**. A shift in emission seems to be influenced by the presence of $\pi - \pi$ interactions between neighboring TPTZ ligands.

Table S10. Spectroscopic data (fluorescence and lifetimes) for **1-9** at 365 nm (298 K).

Compound	O/N Ligand	$\lambda_{\text{em}} / \text{cm}^{-1}$	$\tau / \mu\text{s}$ (365 nm exc)
1	Br-BDC/ TPY	20284, 19455, 18622, 17794	49.89, 119.02 (84%)
2	Cl-BDC/ TPY	20284, 19417, 18622, 17794	35.40, 86.72 (77%)
3	Br-BDC/ TPTZ	20364, 19531, 18692, 17889	66.12, 111.89 (60%)
4	Cl-BDC/ TPTZ	20325, 19493, 18692, 17825	58.89, 108.44 (61%)
5	I-BDC/ TPTZ	-	-
6	Me-BDC/ TPTZ	20325, 19493, 18692, 17857	32.78 (74%), 72.54
7	TDC/ TPTZ	20367, 19493, 18692, 17794	35.16 (7%), 11.15 (66%), 3.87 (28%)
8	TDC/ TPY	20202, 19342, 18484, 17637	35.69 (18%), 116.39 (79%), 7.45 (2%)
9	TDC/ Cl-TPY	20284, 19417, 18587, 17762	41.75 (33%), 85.94 (54%), 1.58 (12%)